Hybrid silica micro-particles with light-responsive surface properties and Janus-like character

Polymer Chemistry

ARTICLE

Hybrid silica micro-particles with light-responsive surface properties and Janus-like character

Received 00th January 20xx,
Accepted 00th January 20xx

DOI: 10.1039/x0xx00000x

www.rsc.org/

A. Romano,[a] M. Sangermano[a]† , E. Rossegger,[b] I. Mühlbacher,[b] T. Griesser,[c] M. Giebler,[b] G. Palmara,[a] F. Frascella,[a] I. Roppolo,[a] and S. Schlögl[b]

The present work highlights the synthesis and post-modification of silica-based micro-particles containing photo-responsive polymer brushes with photolabile *o*-nitrobenzyl ester (*o*-NBE) chromophores. For the synthesis of the polymer brushes, two different procedures were pursued. In the first approach, an amino-functional organosilane was covalently attached onto the silica surface followed by the thermal coupling of a mono-functional epoxy monomer containing *o*-NBE groups. In the second approach, a long wavelength absorbing Norrish Type I photoinitiator bearing functional trialkoxy silane moieties was immobilized across the silanol groups of the silica surface by condensation reaction. Upon visible light exposure, the photoinitator was homolytically cleaved and the formed radicals acted as anchor points for a grafting-from reaction. In particular, an acrylate monomer with *o*-NBE groups was grafted onto the surface of the micro-particles without inducing a premature cleavage of the *o*-NBE links. The photo-induced grafting reaction enabled the formation of photo-responsive polymer brushes within short reaction time and under mild reaction conditions. Once the polymer brushes were formed, the *o*-NBE groups were selectively cleaved upon UV light exposure. Additionaly, particles with Janus-like properties were synthetized by first masking the grafted silica particles through a wax-water pickering emulsion, followed by a selective UV irradiation of the unmasked particles' domain. The formed carboxylic acid moieties were then used for the covalent attachment of a fluorescent biomolecule (Alexa Fluor546 conjugated Protein A). Zeta potential experiments and XPS spectroscopy confirmed the changes in the chemical surface composition of the silica particles prior to and after the surface modification and photocleavage processes. In addition, confocal microscopy images proved the selective anchoring of a fluorescent protein onto the surface of UV irradiated particles surface areas, giving rise to the versatility of *o*-NBE chemistry for the fabrication of light-responsive hybrid particles.

Introduction

In the last decades, functional micro and nano-sized particles have gained increased attention and expanded their range of application in numerous fields [1–6]. Whilst several studies describe particles, which are either inorganic or polymeric in nature, [6,7] there is a promising hybrid type. Those so-called "hairy" particles typically have an inorganic core, on which polymer chains are covalently grafted [8]. They have received tremendous interest due to their potential to design systems with unique and unprecedented properties [6,7,9].

For instance, when the ~~"hairy"~~ polymer~~s~~ brushes are comparable in size to the inorganic core structure, the particles exhibit interesting features for biomedical applications, as they behave like "soft" objects similarly to biological materials such as blood cells or organ tissues [10]. Moreover, the ~~"hairy"~~ polymeric shell surface can be exploited in order to change the interface properties of the particles in a surrounding environment (e.g. enhancing the dispersion in solvents or polymers) and to impart stimuli-responsive properties on the particles' shells [11,12]. Regarding the synthesis strategies, ~~hairy~~ polymer brushes ~~particles~~ are mainly ~~prepared~~ grown onto the particles surface via two different approaches: (i) grafting-to and (ii) grafting-from procedures [13]. In a grafting-to approach, the polymer chains are directly grafted onto the surface via a chemical reaction between surface functionalities of the particles and terminal groups of polymers [13,14]. This approach is also typically exploited for grafting of proteins. By properly selecting the molecules to graft, it is possible to achieve a precise control of the surface functionalization and related surface properties. On the other hand, the steric hindrance of the macromolecules as well as the low probability of reaction (only terminal groups are used for anchoring) do not allow a densely-packed functionalization.

In contrast, the grafting-from strategy exploits a direct polymer chain growth from the surface by following a surface-initiated polymerization. In the first step, initiating species (i.e. a photoinitiator) are immobilized onto the surface, from which

[a] *Department of Applied Science and Technology, Politecnico di Torino, Corso Duca degli Abruzzi 24, 10129 Torino, Italy.*
[b] *Polymer Competence Center Leoben GmbH, Roseggerstrasse 12, A-8700 Leoben, Austria.*
[c] *Institute of Chemistry of Polymeric Materials, Montanuniversitaet Leoben, Otto Glöckel-Strasse 2, A-8700 Leoben, Austria.*

† E-mail: marco.sangermano@polito.it

Electronic Supplementary Information (ESI) available: NMR spectra of *o*-NBE monomes, XPS and FT-IR data of silica particles prior to and after modification. See DOI: 10.1039/x0xx00000x

the polymerization process starts. Since the polymer chains are grown from the surface, it is possible to achieve higher grafting densities and longer grafted polymeric chains [13,14]. By employing reversible addition–fragmentation chain-transfer polymerization (RAFT) or atom transfer radical polymerization (ATRP), also a good control of the molecular weight polydispersity can be achieved [15–18].

Introducing stimuli-responsive features to hybrid particles gives the fascinating possibility to remotely control their properties at a micrometric or nanometric scale [19,20]. Many types of stimuli-responsive micro and nano-sized particles and their application in different fields have been reported in literature [20]. Among the various stimuli, light-responsive systems particularly benefit from the high level of selectivity and allow a spatial and temporal control of material properties [21]. In this context, the employment of ortho-nitrobenzyl (*o*-NB) alcohol chromophores represent a versatile route to impart light-responsive features to polymer ~~networks~~materials. First applications of *o*-NB alcohol moieties as photolabile groups in polymer chemistry involved the fabrication of UV-sensitive photoresists. Over the past years, they were adopted as photocleavable crosslinkers for light-triggered drug delivery or as photocleavable junctions in copolymer blocks [22–35]. Advancing from bulk properties, the photo-sensitive nature of *o*-NB alcohol groups was further used to opto-regulate the surface chemistry of polymers [36–38]. Examples are the fabrication of polyelectrolyte multilayers or the photopatterning of micro and nano-arrays for spatially controlled protein immobilization and cell culture [39–42]. Other interesting applications include photocleavable self-assembled monolayers (SAMs) and optical devices [43–46].

In previous works, we synthetized selected monomers containing ortho-nitrobenzyl ester (*o*-NBE) chromophores to prepare functional and photo-responsive polymer coatings. In particular, we exploited the photosensitive nature of *o*-NBE groups in both synthesis and post-modification of polymer ~~networks~~ materials~~–~~[21,47–54]. *o*-NBE moieties were also widely proposed as efficient moieties for the synthesis of hybrid or polymeric particles with light-responsive features [55–58]. However, most of the reported systems require synthesis routes, which suffer from long reaction times and often need harsh conditions and/or catalysts [55,59,60]. These drawbacks can be overcome by applying photo-grafting reactions, which proceed under milder conditions and allow a better control over the process [14,61].

In this work, we apply a photo-induced grafting-from reaction to create photo-responsive polymer brushes onto silica surfaces (Figure 1a). First, a long wavelength absorbing Norrish Type I photoinitiator with functional trialkoxy silane moieties (TMESI²-BAPO) is attached onto the silica surface by condensation reaction. In a second step, the surface-bound TMESI²-BAPO is homolytically cleaved upon visible light exposure, generating radical species, which acts as initiators for the photopolymerization of acrylate monomers containing *o*-NBE groups. In previous works, we used attached TMESI²-BAPO on either glass or silica surfaces followed by subsequent grafting-from reaction of conventional acrylate monomers [61,62]. Along with the photo-grafting route, we pursued a second modification approach using the ring opening of epoxy moieties containing o-NBE moieties with amine groups (Figure 1b).

~~Advancing from polymer brushes with permanent properties, in this work we demonstrate the facile synthesis of photo-responsive polymer brushes by a visible light triggered grafting-from reaction without premature cleavage of the *o*-NBE links~~.

The photolabile links are then selectively cleaved upon subsequent UV exposure yielding free carboxylic acid groups, across which a fluorescent protein was immobilized in a post-modification process.

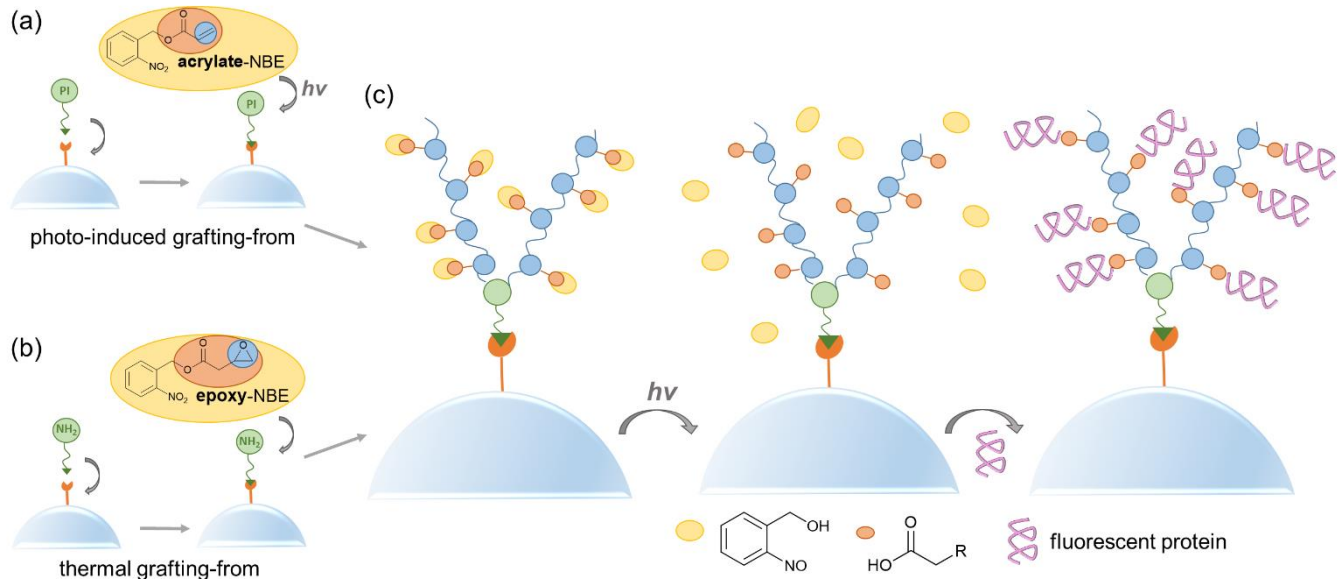

Figure 1 – Synthetic procedures for the fabrication of photo-responsive hybrid particles. (a) Immobilization of TMESI²-BAPO onto the silica surface and visible light induced grafting-from of a mono-functional acrylate with *o*-NBE groups. Photo-responsive polymer brushes are obtained, which yield free carboxylic groups upon subsequent UV exposure. (b) Immobilization of an amino-

functional organosilane onto the silica surface and ring opening reaction of the $–NH_2$ moieties across an epoxide comprising *o*-NBE groups. Selective cleavage of the *o*-NBE chromophore upon UV light irradiation yields free carboxylic acids groups. In both cases, the –COOH groups are exploited for the subsequent immobilization of the fluorescent Alexa-546 protein.

~~Along with the photo-grafting route, we pursued a second modification approach using the ring opening of epoxy moieties with amine groups (Figure 1b). In the first step, an amino-functional organosilane is attached onto the surface of the silica particles by condensation reaction. The surface $–NH_2$ groups are then exploited as reactive anchor groups for coupling and grafting of a mono-functional epoxide monomer with photolabile *o*-NBE groups. Upon UV irradiation, the cleavage of the *o*-NBE chromophores yields –COOH groups, which are used for the immobilization of the fluorescent Alexa-546 protein.~~

In a last step we showed the possibility to exploit the photo-responsive nature of *o*-NBE polymer brushes for the synthesis of particles with Janus-like properties. Janus particles (JPs) are a class of particles, which possess an asymmetrical nature by showing two or more faces with directionally different physical and/or chemical properties [63,64]. Different methodologies are reported in literature for the fabrication of Janus particles, that rely on a first immobilization of the particles, followed by a selective modification of the unmasked particles domains [14,61,63–69]. In a recent work[63], Razza and co-workers proposed a fast and efficient synthetic route that combined an emulsion-assisted immobilization (i.e, Pickering emulsion) of silica particles with thiolate functional groups, followed by a photochemical formation of PEG polymer brushes onto the unmasked particles areas. By reverting the synthetic steps, in this work we obtained the Janus-like character by first immobilizing the grafted silica particles at a wax-water pickering emulsion interface, followed by a selective UV-cleavage of the *o*-NBE moieties onto the unmasked particles' surface domain. Confocal microscopy images proved the selective anchoring of the fluorescent protein only onto the UV irradiated areas, confirming the successful formation of particles with Janus-like properties and with very fast reaction rate (only 1 minutes of UV irradiation). This last result showed the potentiality of *o*-NBE chemistry also for the synthesis of particles with asymmetrical properties, demonstrating the wide range of potential applications of *o*-NBE chemistry in the design of functional and stimuli-responsive hybrid particles.

Results and Discussion

Silanization of silica microparticles

For the synthesis of the hybrid particles, conventional silica microparticles with a d_{50} value of 1.0 µm were employed. To increase the number of silanol groups (Si-OH) on their surface and to remove any organic contaminants, the silica particles were pre-treated by a RCA-SC1 chemical treatment protocol using hydrogen peroxide and ammonium hydroxide. In the FTIR spectra of the pre-treated particles, a distinctive absorption band at 758 cm^{-1} is observed, which is related to the presence of silanol moieties (Figure S1, in ESI). The silanol groups were further exploited to attach functional organosilanes by condensation reaction, which was carried out under anhydrous conditions and in the absence of any catalyst. Under these conditions the organosilane is hydrolyzed by water that is pre-adsorbed on the silica surface and hydrogen bonds are formed between the hydrolyzed silane and the surface silanol groups on the silica. A subsequent thermal treatment of the particles leads to the formation of siloxane bonds by condensation reaction. Along with a covalent attachment onto the particle surface, the trimethoxysilanol groups might undergo grafting reactions yielding oligolayers. However, under the applied conditions, it is expected that the formation of oligolayers plays a minor role. The covalent attachment of TEMSI²-BAPO and 3-APTMS onto the pre-treated silica particles is confirmed by TGA and XPS experiments. Figure 2a shows the weight loss of pristine and modified silica particles as obtained from TGA experiments. Untreated silica microparticles comprise a weight loss of 5%, which is attributed to surface dehydration. After surface modification, a higher weight loss is observed giving rise to the successful coupling of the organosilanes. In particular, the additional weight loss amounts to 1.1% and 2% for particles modified with TEMSI²-BAPO and 3-APTMS, respectively.

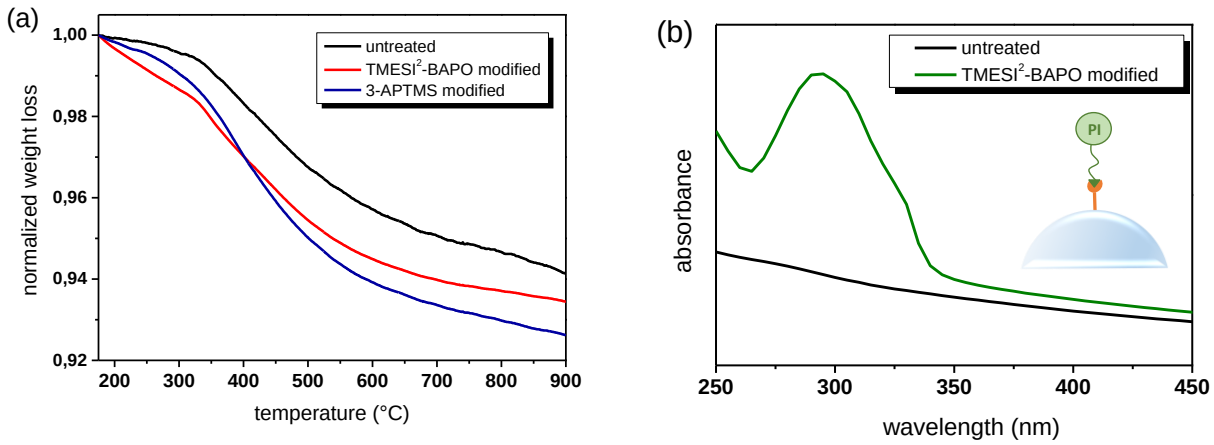

Figure 2 – (a) TGA curves of silica particles prior to and after the modification with TMESI²-BAPO and 3-APTMS, respectively. (b) UV-Vis spectrum of untreated silica particles in comparison to silica particles modified with TMESI²-BAPO. The particle concentration amounted to 0.15 mg mL^{-1} in absolute ethanol.

To get a deeper insight into the chemical surface composition, XPS spectra were taken from modified silica particles. The attachment of TEMSI²-BAPO is confirmed by the appearance of the characteristic phosphorous photoemission at 133.4 eV (P2p3 signal), whilst the immobilization of 3-APTMS is related to a distinctive nitrogen photoemission at 401.8 eV (Figure S2a and b in ESI).

The TEMSI²-BAPO functionalized particles further exhibit the characteristic absorption profile of the free trimethoxysilyl-functionalized photoinitiator, which is clearly absent in the UV-Vis spectrum of the untreated silica particles (Figure 2b) [61]. It should be considered that TEMSI²-BAPO benefits from an extended absorption window (> 400 nm), but the modification yield of the particles is too low to observe the long wavelength absorption bands in the UV-Vis spectrum of the modified particles.

Formation of photo-responsive polymer brushes

A visible light promoted formation of polymer brushes was carried out by exploiting the surface-bonded TMESI²-BAPO photoinitiators. The photo-induced grafting-from procedure is of particular interest because it allows a photo-induced formation of polymer brushes, taking advantage of the high time-spatial control and mild reaction conditions of the light triggered reactions (Figure 3). In previous works, TMESI²-BAPO was immobilized onto inorganic particles to act as photo-reactive anchor for photo-induced grafting-from surface modification strategies [61,70] or for the synthesis of low migratable photoinitiators [71,72]. BAPO derivatives present several interesting features including a relatively high thermal stability (> 100 °C), extended storage stability, and a photolysis which yields a total of up to four radicals, with the phosphinoyl radical about 1000 times more reactive than the acyl radicals.

Moreover, in our synthesis route the extended absorption window of TMESI²-BAPO enables the visible light induced photo-grafting of photolabile acrylate monomers without premature cleavage of the UV sensitive *o*-NBE chromophores.

Upon visible-light irradiation, TMESI²-BAPO undergoes a homolytic bond cleavage and forms up to phosphinoyl radicals that ideally promote the growth of two polymer chains from a single photoinitiator anchoring site[73–75] (Figure 3).

Furthermore, this system is ideal for the formation of polymer brushes as the acyl radicals, which are generated at the same time and are released in the solvent, are significantly less reactive. Thus, the amount of homopolymers generated as side-products can be reduced and are easily removable [14].

In the current study, (2-nitro-1,4-phenylene) (methylene) acrylate (mono-acrylate-**NBE**) was employed as photosensitive monomer for the grafting-from reaction. Mono-acrylate-**NBE** was obtained by an esterification of 2-nitrobenzyl alcohol with acryloyl chloride (Figure 4a). The one-step synthesis afforded the product in 70% of the theoretical yield and ^{1}H NMR spectrum was in accordance with the proposed structure (Figure S3 in ESI).

TGA measurements clearly show that the grafting reaction can be controlled by the irradiation conditions. At an irradiation intensity of 350 mW/cm², the photo-grafted particles exhibit an additional mass loss of 0.6% compared to the TMESI²-BAPO modified ones (Figure 4c). Although the absolute value of this mass loss might seem low, the calculated amount of polymer grafted per unit area was 3 mg/m², which is in good agreement with other "photo-grafted-from" polymer brushes reported in literature (7-10 mg/m²) [61].

However, by reducing the light intensity to 20 mW/cm², the mass loss was comparable to the TMESI²-BAPO modified particles. The high sensitivity of the photo-activated reaction to exposure dose can be explained by the quantum yield of BAPO and its derivatives, which is lower in the visible light region compared to the UV spectral region.

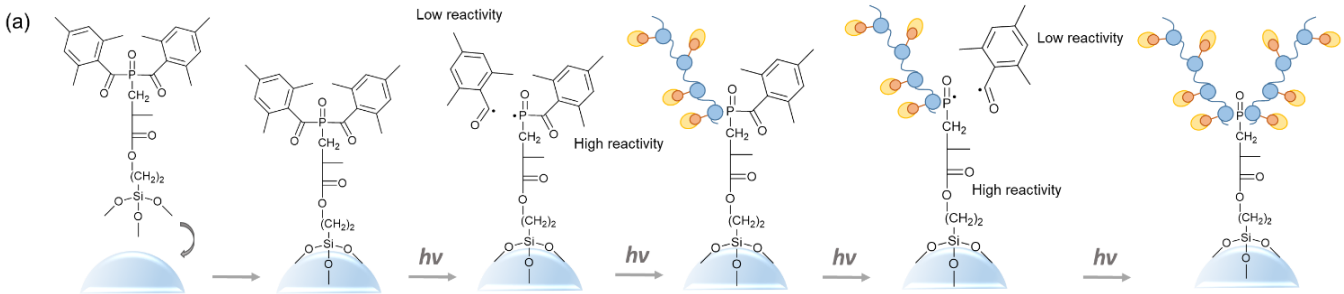

Figure 3 – (a) Schematic representation of the visible light-induced grafting-from reaction exploiting surface-bond TMESI²-BAPO as initiating species and mono-acrylate-**NBE** as reactive monomer.

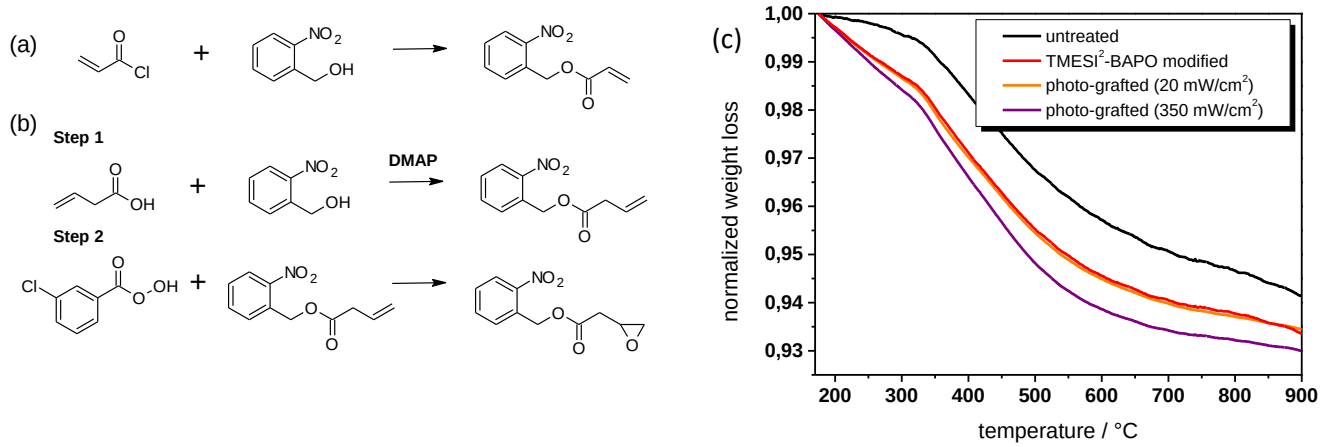

Figure 4 – Synthesis of (a) mono-acrylate-**NBE** and (b) mono-epoxy-**NBE**. (c)TGA curves of untreated, TMESI²-BAPO modified and photo-grafted silica particles. The grafting-from process was carried out upon visible light exposure either at 20 mW/m² or 350 mW/m² for 4 h.

This is also demonstrated by the UV-Vis spectra of TMESI²-BAPO modified silica particles, in which the long wavelength absorption region is not visible (Figure 2b).

Thus, relatively high light irradiation doses were required to obtain detectable grafting yields. In addition, it should be noted that mono-acrylate-**NBE** showed generally a lower efficiency in the grafting yield compared to other acrylate monomers such as acrylic acid. As previously reported, both in radical controlled polymerization and in thiol-ene click reactions [53,76], *o*-NBE groups retard radically promoted reactions and reduce the overall reactivity compared to conventional acrylate systems. A further increase of the amount of grafted monomer was limited by several factors. An increase of the exposure dose also promoted a slight cleavage of the *o*-NBE due to the partial overlapping at the border of the visible light source's emission and the *o*-NBE absorption window. However, using a longer wavelength cut-off filter (i.e. $\lambda < 420$ nm) would further reduce the quantum yield of TMESI²-BAPO and would require substantially prolonged irradiation times.

In the second approach, photo-responsive polymer brushes were obtained by exploiting a direct epoxy-amine coupling reaction between the free $-NH_2$ groups of 3-APTMS modified silica particles and the epoxy group of (2-nitrophenyl) (methyl) (2-(oxiran-2-yl)acetate) (mono-epoxy-**NBE**). Mono-epoxy-**NBE** was achieved by a two-step reaction involving in the first step a *Steglich* esterification of 2-nitrobenzyl alcohol with 5-hexynenoic acid (Figure 4b). The formed intermediate (2-nitrophenyl) (methyl 3-butenoate) was reacted with 3-chloroperbenzoic acid to give mono-epoxy-**NBE** with good yields (65%). The ^{1}H NMR spectrum was in accordance with the proposed structure (Figure S4 in ESI).

The ring opening reaction of epoxy moieties with amino groups typically proceeds via a step-growth polymerization mechanism involving a nucleophilic attack of the amine to the less sterically hindered carbon of an oxirane ring (Figure 5a).

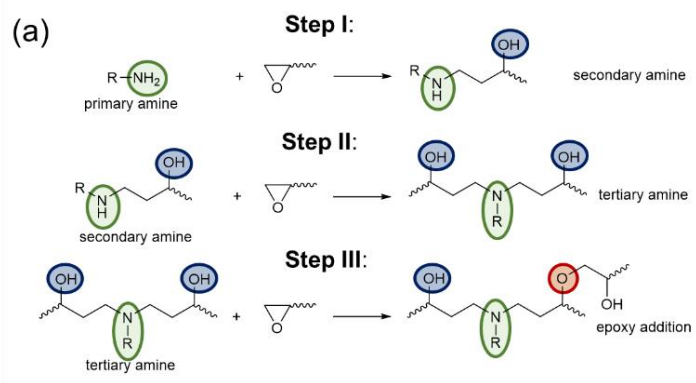

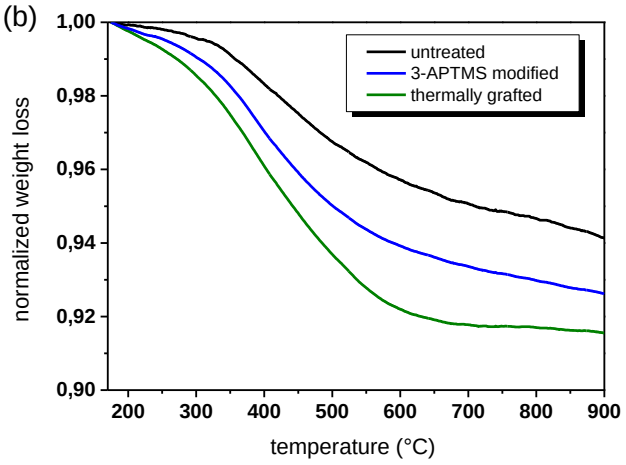

Figure 5 – (a) Schematic representation of the thermally induced grafting-from reaction exploiting surface-bonded 3-APTMS as initiating species and mono-epoxy-**NBE** as reactive monomer. (b) TGA curves of untreated, 3-APTMS modified and thermally grafted silica particles.

In the case of primary amines, the addition reaction yields a secondary amine and a hydroxyl group [77,78]. The resulting secondary amine, which is more sterically hindered than the primary amine, reacts then with another oxirane ring, creating an additional hydroxyl group and a tertiary amine. Eventually, the hydroxyl groups generated by the reaction between the secondary amine and epoxide group will result in the formation of ether linkage. This reaction, generally known as etherification, competes with the epoxy-amine curing reaction and takes place after consumption of amine hydrogens and if epoxide groups are in excess [78].

The thermally grafted silica particles exhibited an additional mass loss of about +0.6% compared to the 3-APTMS modified ones, which is in a similar range as the photo-grafted particles (Figure 5b). However, whilst the thermally grafting requires 10 hours at 65 °C, the photo-grafting is accomplished within 4 hours of visible light irradiation at room temperature.

Photo-induced cleavage of photo-responsive polymer brushes and post-modification

A controlled change of polarity and reactivity of the modified silica particles was carried out by selectively cleaving the *o*-NBE moieties in the grafted polymer brushes upon UV exposure. The UV induced cleavage of *o*-NBE chromophores yields polymer brushes with free carboxylic acids anchored to the particle's surface, whilst nitroso benzaldehyde products are ideally released in the solvent phase. To characterize the light-induced changes in the surface properties, zeta potential measurements and XPS spectroscopy were carried out. For a better understanding of the changes in polarity, contact angle measurements were performed on glass slides that were modified with a procedure similar to the one adopted for the silica particles (see experimental part in ESI).

The zeta potential curves for the two different grafting-from procedures are plotted in Figure 6. Zeta potential values reflect the overall particle charges that depend on both the dissociation of functional surface groups into cationic or anionic species, and the adsorption of ions onto the particles' surface [79]. For the untreated particles, the higher negative zeta potential values at higher pH (-45 mV at pH = 4) reflect the particles' silanol groups, which dissociate into Si-O^- anions [80]. For the photo-induced grafted-from particles only slight differences in the zeta potential curves versus pH values are observed (Figure 6a). Due to the coupling of $TMESI^2$-BAPO, the silanol groups of the silica particles are partly occupied by the larger and more hydrophobic photoinitiator molecules. The higher hydrophobicity is also confirmed by contact angle measurements (Table 1), showing an increase of the water contact angle from 23 to 58° due to the attachment of $TMESI^2$-BAPO. The lower amount of dissociable species might explain the shift of the zeta potential to lower negative values (-35 mV at pH = 4). The photo-grafting of mono-acrylate-**NBE** leads to a further shift of the zeta potential to lower negative values. Here it has to be considered that the photo-grafted polymer brushes contain dissociable nitro groups but also largely cover the remaining free surface silanol groups, which leads to a further shift of the zeta potential to lower negative values. Subsequent UV-induced cleavage of the *o*-NBE groups in the polymer brushes yields free carboxylic acid groups, which are deprotonated at higher pH values. In the deprotonated state, preferentially water molecules adsorb on the silica surface instead of (OH^-) ions, which leads to a further decrease of the zeta potential to lower negative values. The UV induced formation of polar cleavage products is also confirmed by water contact angle experiments giving rise to a decrease in the water contact angle from 62 to 48° (Table 1).

For the thermally grafted particles exploiting the epoxy-amine coupling reaction, the attachment of 3-APTMS leads to a strong shift of the isoelectric point (IEP) compared to the untreated silica particles (Figure 6b). The shift to higher values clearly indicates the presence of primary amino groups that in aqueous solution tend to dissociate to -NH_3^+ cationic species, leading to positive zeta potential values at pH values higher than 9.5. In addition, the coupling of the amino-functional silane facilitates a distinctive increase in the water contact angle from 23 to 50° as the highly polar silanol groups are consumed during the condensation reactions (Table 1).

Table 1 – Water contact angles of glass sides prior to and after modification and photochemical or thermal grafting reaction

samples photo-grafting	water contact angle / °	**samples thermal grafting**	water contact angle / °
untreated	23 ± 10	untreated	23 ± 10
$TMESI^2$-BAPO	58 ± 5	3-APTMS	50 ± 5
grafted	62 ± 5	grafted	63 ± 5
UV cleaved	48 ± 5	UV cleaved	35 ± 5

Along with zeta potential and contact angle measurements, XPS experiments were performed to characterize the change in the chemical surface composition of the grafted particles prior to and after the cleavage of the *o*-NBE chromophores. To get a clearer picture on the cleavage, high-resolution C1s spectra were recorded and after deconvolution three different peaks were detectable: C-C/C-H peak at 284.9 eV; C-N/C-O/C-COOH peak at 286.3 eV and O-C=O ester groups at 288.6 eV (Figure 7 and Figure S5 in ESI) [60,81,82]. The relative carbon atomic percentages of each peak were calculated by normalizing the corresponding area to the overall C1s peak ($C1s_{bond}/C1s_{TOT}$) and the results are summarized in Table 2.

For the photo-grafted particles, a distinctive increase of the area related to C-COOH groups (peak at 286.3 eV) is observed after UV exposure (Figure 7b), which indicates the formation of free carboxylic acid groups (-COOH). The increase of the C-COOH groups is also accompanied by a slight increase of peak

related to the ester groups (O-C=O) from 10.7% to 17.7% ($C1s_{(O-C=O)}/C1s_{TOT}$).

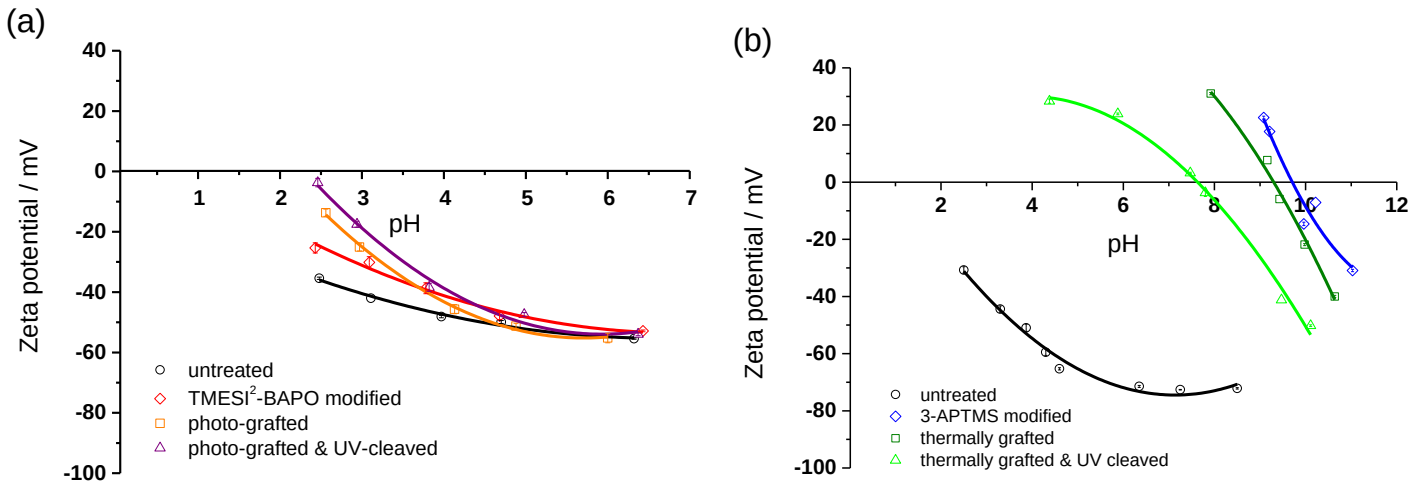

Figure 6 – Zeta potential curves as a function of the pH value from (a) photo-grafted and (b) thermally grafted silica particles.

Table 2 – Calculated peak areas ($C1s_{bond}/C1s_{TOT}$) of different C-linked groups as obtained from deconvoluted high-resolution C1s spectra.

Binding energy (eV)	Chemical groups	photo-grafted (at%)	photo-grafted & UV cleaved (at%)	thermally grafted (at%)	thermally grafted & UV cleaved (at%)
284.9	C-C/C-H	75	57	56	38
286.3	C-O/C-COOH/C-N	14	26	35	44
288.6	O-C=O	11	17	9	22

However, it should be noted that the signal of the O-C=O ester (288.6 eV) from the o-NBE group is partly overlapping with the free carboxylic acid HO-C=O species (289.1 eV), which makes the interpretation and quantification difficult for this peak area. In contrast, a clear distinction between the exposed and non-exposed grafted particles is instead evident in the high-resolution N1s spectra in Figure 7c, as the -NO_2 peak disappears at 406.5 eV. The XPS results confirm that mono-acrylate-**NBE** monomer was first successfully photo-grafted onto the silica particles, and subsequently cleaved upon UV light irradiation under the formation of free carboxyl acid moieties [60,83].

Thermally grafted silica particles follow the same trend but with a higher increase of the O-C=O area (Table 2 and Figure S5 in ESI). This might be a consequence of the higher amount of grafted monomers for those particles (see TGA curves in Figure 4c and 5b). This result might also depend on the lower overlapping effect of the ester groups for the thermally grafted particles, because of the absence of ester groups in the 3-APTMS silanes structure that are instead present in the TMESI²-BAPO molecules.

Summing up, zeta potential measurements, contact angle as well as XPS data confirm the ~~controlled~~ formation of free carboxylic acid moieties by UV-induced cleavage of the polymer brushes grafted photochemically or thermally.

The formed –COOH groups were further used to selectively attach labelled proteins giving rise to the versatility of the photo-responsive polymer brushes. In particular, the carboxylic groups formed by the photo-cleavage of the *o*-NBE groups were used as anchor points to attach an Alexa-546 conjugated fluorescent protein. This allowed us, not only to further confirm the availability of surface active moieties, but also to demonstrate that these functional groups can be exploited for the immobilization of biomolecules, such as proteins, which is of primary interest in biomedical applications (e.g. biosensors, microarrays, lab-on-a-chip) [84]. The adopted procedure followed an EDC-NHS protocol as described in the experimental section. For both grafting-from procedures, the confocal microscopy images are provided in Figure 8. For grafted particles, no fluorescent signal was detected after EDC-NHS protocols and protein immobilization step, because in the absence of free –COOH groups the proteins have not been covalently attached to the polymer brush (Figure 8a and 8c). The results also indicate that the applied protocol is highly efficient in removing any non-covalently bonded proteins.

However, a clear fluorescent emission can be detected for thermally as well as photochemically grafted particles which have been additionally illuminated with UV-light (Figure 8b and 8d). The results evidence that an effective immobilization of the fluorescent proteins does only occur onto the UV irradiated silica particles, demonstrating the light induced carboxylic acids formation and the active role of the *o*-NBE chromophores in the post-modification process.

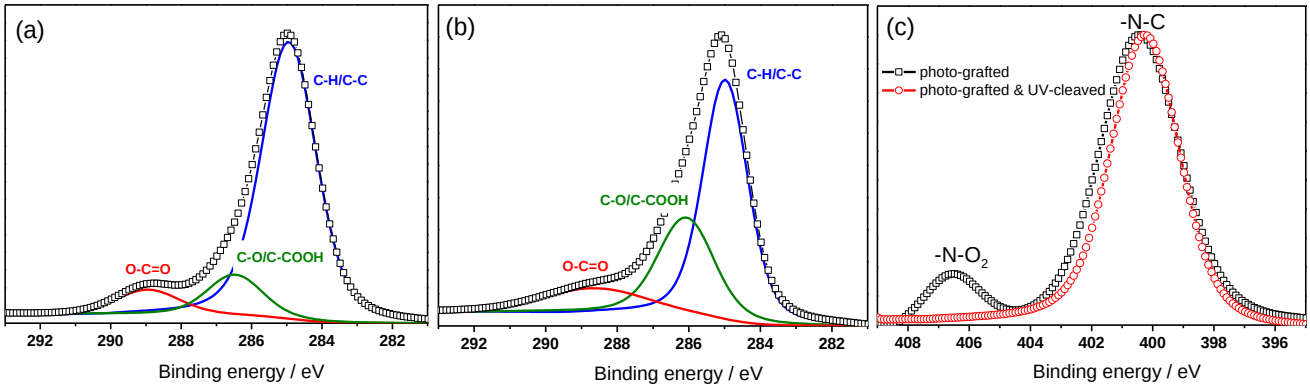

Figure 7 – Deconvoluted high-resolution C1s spectra of photo-grafted silica particles (a) prior to and (b) after UV-induced cleavage. Deconvoluted high-resolution N1s spectra (c) of photo-grafted silica particles prior to and after UV-induced cleavage.

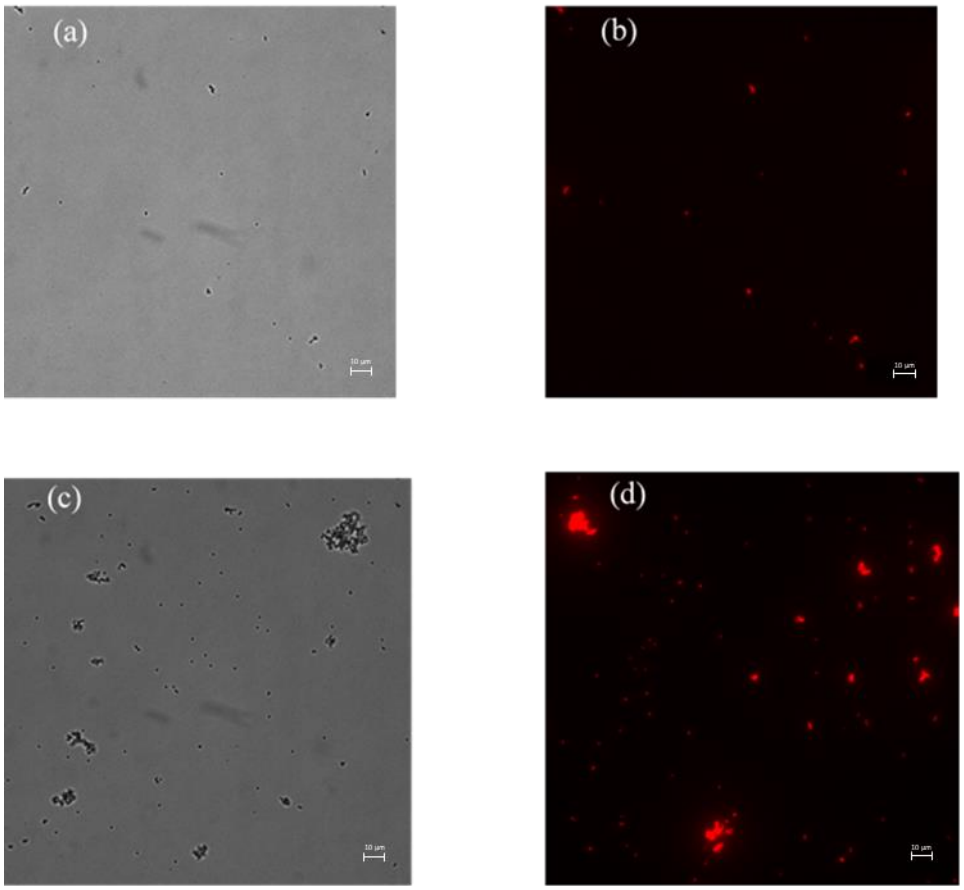

Figure 8 – Confocal microscopy images: (a) Photo-grafted non-cleaved particles, on which no proteins were anchored and thus no fluorescent signal was detected after EDC-NHS protocols. (b) Photo-grafted and photo-cleaved particles, on which a fluorescent signal was detected after EDC-NHS protocols giving rise to the covalent attachment of the fluorescent proteins. (c) Thermally grafted non-cleaved particles, on which no proteins anchoring was detected after EDC-NHS protocol. (d) Thermally grafted and

photo-cleaved particles, on which the fluorescent signal was detected after EDC-NHS protocols evidencing the anchoring of the fluorescent proteins. The scale bar is 10 µm.

In a last step, we fabricated Janus-like particles exploiting a selective UV cleavage of the o-NBE moieties onto the thermal and photo-grafted silica particles surface. The synthesis procedure involved a prior step in which the particles were partially masked to expose only one domain to the UV irradiation, therefore obtaining physical and chemical asymmetry onto the overall particle surface. In this approach, a solid particles' stabilized emulsion was prepared by mixing a solution of melted paraffin (oil phase), deionized water (water phase) and grafted silica particles as emulsion stabilizer. During the emulsification, the silica particles spontaneously migrate to the oil/water interface to stabilize the emulsion (Figure 9 a, b and c). Once the solution is cooled down, the paraffin phase solidifies blocking the particles at the oil/water interface and thus, small wax droplets are obtained (Figure 9 a and b). In this way, a partial masking of the particles was obtained (Figure 9 c). In a further step, the water-colloidosomes solution was irradiated by UV light, therefore promoting the o-NBE cleavage of the unmasked surface areas. The magnification images of confocal microscope in Figure 9 d, e and f, clearly show the Janus character of the irradiated particles, with only one domain further functionalized with fluorescent proteins, and upon only one minute of UV irradiation.

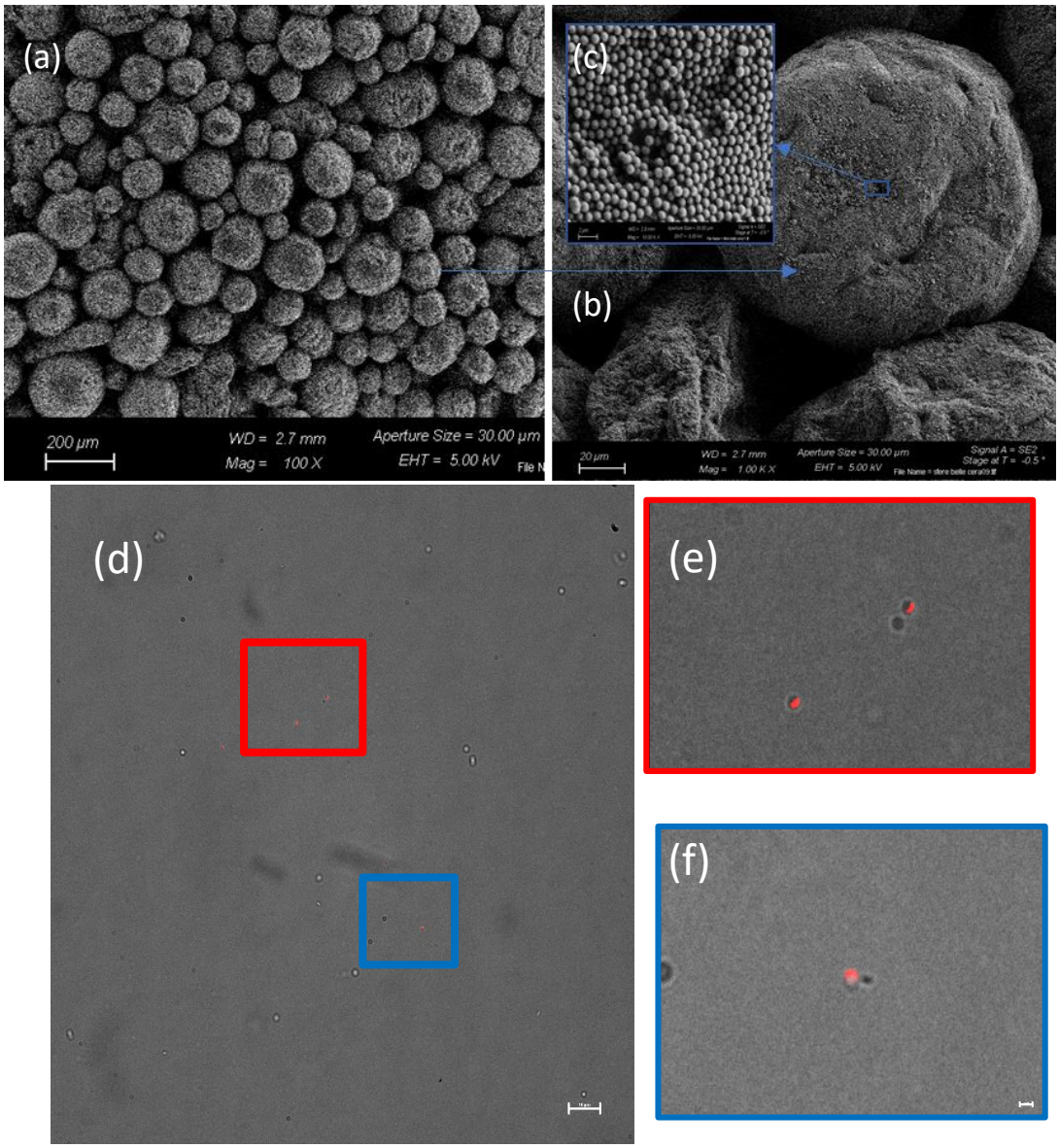

Figure 9 – FE-SEM micrographs of the emulsion-assisted masking. (a) Overall view of the collected wax droplets stabilized by photo-grafted silica particles after wax solidification (colloidosomes), the scale bar is 200 µm (b) Magnification of colloidosome droplet. The scale bar is 20 µm (c) Magnification of the colloidosome interface with the encapsulated photo-grafted silica particles, the scale bar is 2 µm. d, e, f) Confocal microscopy images of UV-cleaved Janus-like particles (1 minutes of UV irradiation). The scale bar

is 10 μm. The red and blue squares highlight the particles which are magnified out of in Figure 9e and 9f, respectively. Asymmetrical immobilization of the fluorescent proteins only onto the irradiated areas of the hybrid silica particles is clearly visible. The scale bar is 1 μm

However, an increase of the irradiation time up to 5 minutes caused the o-NBE cleavage also of the masked areas. We suppose that the UV cleavage of the covered areas is caused by the UV light penetration through the silica core at prolonged UV irradiation dose. Despite this limitation, the proposed method shows a very promising and fast synthetic route (only 1 minute of UV irradiation) for the synthesis of particles with Janus-like properties, and at the best of our knowledge represents the first adoption of o-NBE moieties for the synthesis of particles with asymmetric properties. This result paves the way to different applications of this new class of light-responsive particles, as for instance as photo-responsible emulsion stabilizers or for obtaining asymmetric and complex nanostructured domains. In future works we will extend this approach to other inorganic particles and examine different possible applications of this promising class of hybrid light-responsive particles.

Conclusions

In this work, we carried out two different grafting-from procedures for the synthesis of photo-responsive hybrid silica micro-particles. As first approach, a photochemical synthesis route was employed for the formation of photo-responsive polymer brushes, exploiting a radical mediated grafting reaction of acrylate monomers comprising *o*-NBE chromophores. TMESI^2-BAPO was anchored on the surface of silica particles by condensation reaction and subsequent exposure with visible light led to the formation of starting radicals for the chain growth reaction of mono-acrylate-**NBE**. In the second approach, a nucleophilic ring opening reaction of epoxy groups with primary amines was applied to immobilize *o*-NBE monomers on the surface of silica micro-particles. An amino-functional silane (3-APTMS) was anchored onto the silica surface by condensation reaction and the free amino groups were exploited to covalently attach an epoxy monomer bearing an *o*-NBE group. In both strategies no toxic substances have been employed, whilst the photochemical synthesis route was carried out under mild conditions and at room temperature. Although mono-acrylate-**NBE** monomers suffer from a low reactivity in radical mediated polymerization, the thermogravimetric analysis showed adequate performance for the photochemical synthesis in terms of grafted-from polymer brush versus reaction time. However, the amino-epoxy reaction appeared instead more “scalable” if higher grafting efficiency was required. Once the polymer brushes were formed, the *o*-NBE groups of the polymer brushes were exploited to change the surface properties upon UV-light as external trigger. Zeta potential measurements and XPS spectroscopy demonstrated that UV-induced changes in particles’ physical and chemical surface properties. Applying a similar synthetic path to glass slides, we further showed that the carboxylic acids, formed as *o*-NBE cleavage products, can be conveniently employed for changing the water contact angle of the polymer grafted surface. Finally, we showed the possibility to exploit the light-responsive nature of the *o*-NBE polymer brushes for the synthesis of silica particles with Janus-like properties, with an easy and fast synthesis route (only 1 minute of UV irradiation). Confocal microscopy images proved the selective anchoring of the fluorescent protein only onto the UV irradiated domains, therefore demonstrating the potentiality of ortho-nitrobenzyl chemistry for the fabrication of light-responsive particles with asymmetrical properties. This could be a starting point for different future applications of those particles, such as photo-responsive emulsion stabilizers or complex and nanostructured domains.

Experimental

Materials and chemicals

Silica microparticles (d_{50} = 1.0 μm, 99.9%) were purchased from Alfa Aesar. Ammonium hydroxide (NH_4OH, 30% solution) and hydrogen peroxide (H_2O_2, 30% solution) were purchased from Carl Roth GmbH Karlsruhe. Ethanol absolute (EtOH, VWR, 99.9%), ethanol (95%), toluene (99.8%), acetonitrile (99.8%), acetone (ACS reagent), (3-aminopropyl) trimethoxysilane (3-APTMS) were purchased from Sigma Aldrich. 3-(trimethoxysilyl)propyl 3-[bis(2,4,6-trimethyl-benzoyl)phosphinyl]-2-methyl-propionate (TMESI^2-BAPO) was synthetized as reported elsewhere [70]. Glass slides were prepared by cutting 2 x 1 cm pieces from microscopic slides (76 x 26 mm cut edges) purchased by Carl Roth GmbH Karlsruhe. The structures of the organosilanes and the photo-responsive *o*-NBE monomers are shown in Figure 1.

For the post functionalization step, 2-(*N*-morpholino)ethanesulfonic acid (MES, 99.5%), sodium chloride (99.5%), 1-ethyl-3-(3-dimethylaminopropyl)-carbodiimide (EDC, 99%), *N*-hydroxysulfosuccinimide sodium salt (sulfo-NHS, 98%), Dulbecco’s phosphate-buffered saline (PBS) and poly(oxyethylene) glycol sorbitan monolaurate (Tween™ 20) were purchased from Sigma-Aldrich and used without further purification. Protein A, Alexa Fluor™ 546 conjugated was purchased from Thermo Fischer Scientific and used according to the manufacturer’s instructions.

Synthesis

(2-nitro-1,4-phenylene) (methylene) acrylate (mono-acrylate-NBE) was synthesized by dispersing acryloyl chloride (4 mL; 49 mmol) with a solution of 2-nitrobenzyl alcohol (5 g; 32mmol) in 50 mL of dry tetrahydrofuran. Triethylamine (4.5 mL, 32 mmol) was dissolved in 50 mL dry tetrahydrofuran and added dropwise to the reaction mixture over 3 hours. The reaction mixture was stirred for 7 h at room temperature and the progress was monitored by TLC. After evaporation of the solvent, the reaction

product, which appeared as a yellowish oil, was dissolved in dichloromethane and extracted with water and saturated Na_2CO_3 solution. The combined organic layers were dried over Na_2SO_4 and the solvent was removed by rotary evaporation. The obtained crude product was further purified by column chromatography (2:1 = cyclohexane:ethyl acetate). The solvent was removed by rotary evaporation and the product was collected as yellowish liquid (50 % of the total theoretical yield). ^{1}H-NMR (δ, 400 MHz, 25 °C, $CDCl_3$): δ = 8.1 (d, 1H); 7.7 (m, 2H); 7.5 (t, 1H); 6.5 (d, 1H); 6.2 (q, 1H); 5.9 (d, 1H) and 5.6 (s, 2H).

(2-nitro-1,4-phenylene) (methylene) (2-(oxiran-2-yl)acetate) (mono-epoxy-NBE) was obtained with a two-step synthesis. In the first step, 3-butenoic acid (3.5 g; 41.5 mmol) was added to a stirred solution of (2-nitrobenzyl alcohol) (5.0 g; 32.6 mmol) in 40 mL dichloromethane. The reaction mixture was cooled to 0 °C and 4-(*N*,*N*-dimethylamino) pyridine (DMAP) (0.8 g; 6.5 mmol) was added. A solution of *N*,*N*'-dicyclohexylcarbodiimide (DCC) (20 g; 96.9 mmol) in 50 mL dichloromethane was placed step-wise to the reaction mixture and stirred at room temperature for 2 h. The obtained product of this reaction step was a yellowish precipitate of (2-nitrophenyl) (methyl 3-butenoate). For further purification, the raw product was washed with H_2O and H_2O/$NaHCO_3$, and dried over Na_2SO_4. After filtration and removal of the solvent under vacuum, a column chromatography (3:1 cyclohexane: ethyl acetate) was carried out. The product amounted at 5.0 g (XX % of the total theoretical yield).

In a subsequent step, an excess of 3-chloroperbenzoic acid (77%) (*m*-CPBA) (36.0 g; 162 mmol) was added step-wise at room temperature to a solution of the synthetized (2-nitrophenyl) (methyl 3-butenoate) (5 g; 22.8 mmol) in 100 mL of dichloromethane. The reaction mixture was stirred at room temperature and after a reaction time of 7 days, a yellowish solution with a white-yellowish precipitate was obtained. The product mixture was then dissolved in dichloromethane and the organic layer was extracted with saturated sodium bicarbonate solution and deionized water. Finally, the solution was dried over Na_2SO_4, filtered and the solvent was removed by rotary evaporation at 30 °C. For final purification a column chromatography (2:1 = cyclohexane:ethyl acetate) was carried out and the yellowish oil was collected after solvent removal under vacuum (45 % of the total theoretical yield).

^{1}H-NMR (δ, 400 MHz, 25 °C, $CDCl_3$): δ = 8.10 (d, *J* = 7.9 Hz, 1H), 7.62 (dd, *J* = 17.8, 7.2 Hz, 2H), 7.50 (d, *J* = 6.9 Hz, 1H), 5.57 (s, 2H), 3.32 (s, 1H), 2.93 – 2.80 (m, 1H), 2.75 – 2.52 (m, 3H).

Surface modification of silica particles

Pretreatment. Silica microparticles were cleaned in order to remove any organic contaminants, and to maximize the surface availability of silanol groups (Si-OH). Following RCA-SC1 chemical treatment protocol, 1 g of silica particles were first sonicated in 100 mL of deionized water (30 min, 50 °C) and then transferred to an open round-bottom flask. 100 mL of hydrogen peroxide (30% solution) and 100 mL ammonium hydroxide (30% solution) were added and the dispersion was heated at 70 °C and stirred (750 rpm) for 1 hour. The particles were then collected by centrifugation and washed 5 times with absolute ethanol by centrifugation/redispersion cycles (3 min, 3000 rpm). The cleaned particles were finally dried overnight at 100 °C under vacuum, in order to remove water residues.

Immobilization of TMESI^2-BAPO. The pre-treated and dried silica particles (600 mg) were dispersed and sonicated for 30 min in 50 mL of anhydrous acetonitrile (99.98%). The dispersion was then transferred to a round-bottom flask. After adding 600 mg of TMESI^2-BAPO, the flask was closed to ensure anhydrous conditions and to avoid any premature condensation among the methoxy silane groups of TMESI^2-BAPO. The mixture was stirred at 500 rpm at room temperature for 48 h. The silanized particles were then collected by centrifugation and washed 5 times with acetone by centrifugation/redispersion cycles (3 min, 3000 rpm), and finally dried at 60 °C under vacuum for 4 hours.

Immobilization of 3-APTMS. The pre-treated and dried silica particles (600 mg) were dispersed and sonicated for 30 min in 50 mL of dried toluene (99.98%). The dispersion was then transferred to a tri-neck-round bottom flask. After adding 600 mg of 3-APTMS, the flask was closed to ensure anhydrous conditions and then connected to a reflux apparatus and to a vacuum/nitrogen line. Additional inert conditions were achieved by flushing the system three times with nitrogen. The dispersion was heated to 80 °C and stirred at 500 rpm for 12 h. Inert and anhydrous conditions were ensured in order to avoid any premature condensation among the methoxy silane groups. The silanized particles were then collected by centrifugation and washed 2 times with toluene and 3 more times with acetone by centrifugation/redispersion cycles (3 minutes, 3000 rpm) and finally dried at 60 °C under vacuum for 4 hours.

Formation of photo-responsive polymer brushes by grafting-from reaction

50 mg of TMESI^2-BAPO silanized particles were dispersed and sonicated for 30 min in 8 mL of acetonitrile. The dispersion was then transferred to a round-bottom flask. After adding 500 mg of mono-acrylate-**NBE**, the flask was closed and inert atmosphere was obtained by flushing the systems three times with nitrogen. Inert atmosphere was particularly important to avoid any oxygen radical inhibition during the photo-grafting process. The dispersion was then stirred at 1000 rpm at room temperature and irradiated for 4 hours with a visible light source, in order to prevent a premature cleavage of the *o*-NBE groups. A medium pressure mercury lamp (Omnicure series 1500) equipped with an optical waveguide was used as light source. An external cut-off filter (Color Glass Filter, 25.4 mm DIA, GG400 cut-off λ < 400 nm) from Newport Corporation was placed between the optical waveguide and the round flask. The intensity amounted to 350 mW cm^2. The photo-grafted particles were then collected by centrifugation and washed 5 times with acetone by centrifugation/redispersion cycles (3 min, 3000 rpm), and finally dried at 60 °C under vacuum for 4 hours.

Formation of photo-responsive organic layers by epoxy-amine coupling reaction

125 mg of 3-APTMS silanized particles were sonicated in 20 mL toluene (99.98%) for 30 min. The dispersion was then transferred to a round-bottom flask. After adding 500 mg of mono-epoxy-**NBE**, the flask was closed, connected to a reflux apparatus and inert atmosphere was obtained by flushing the systems three times with nitrogen. The dispersion was then heated to 65 °C and stirred at 500 rpm under dark conditions (up to 24 h), and left overnight (14 h) at room temperature. The grafted particles were then collected by centrifugation and washed 2 times with toluene and 3 times with acetone by centrifugation/redispersion cycles (3 min, 3000 rpm), and finally dried at 60 °C under vacuum for 4 hours.

Immobilization of fluorescent protein by post-modification of UV exposed hybrid particles

For UV-induced formation of –COOH groups, the modified hybrid particles were dispersed in a Schlenk flask using 50 mg of grafted particles (either photo-grafted or modified by epoxy-amine coupling) in 14 mL of acetonitrile. Inert atmosphere was obtained by flushing the systems three times with nitrogen. The dispersion was then stirred at 1000 rpm at room temperature and irradiated for 30 minutes with a medium pressure mercury lamp (Omnicure series 1500) equipped with an optical waveguide (intensity: UVA = 180 mW/cm^2, UVB = 32 mW/cm^2, UVC = 19 mW/cm^2, UVV 400 = mW/cm^2). The UV-irradiated particles were then collected by centrifugation and washed 5 times with acetone by centrifugation/redispersion cycles (3 min, 3000 rpm), and finally dried at 60 °C under vacuum for 4 hours.

For the subsequent coupling of the fluorescent protein, the carboxylic acid groups formed onto the UV irradiated silica hybrid particles were first "activated" and then conjugated to fluorescent proteins using an EDC/sulfo-NHS protocol. For this purpose, the UV irradiated particles (0.1 mg/mL) were dispersed in 2-(*N*-morpholino) ethanesulfonic acid (MES 0.1 M, pH 4.7) buffer for 15 min. In a further step, the mixture was centrifugated at 5000 rpm for 3 min and the supernatant was removed. The pelleted microparticles were then re-suspended and incubated in a mixture of EDC/sulfo-NHS (4/10 mM) in MES buffer for 15 min on an orbital shaker. At the end of the incubation, the samples were centrifugated as previously described, and the supernatant was discarded. The particles were then re-suspended in phosphate buffered saline (PBS 10 mM, pH 7.3) and placed on an orbital shaker for 5 min. This procedure was repeated two additional times. After the last washing step, the microparticles were re-suspended and incubated overnight in a solution of PBS containing 500 ng/mL of Alexa-546 conjugated Protein A on an orbital shaker. Then, the samples were centrifugated and washed thrice using PBS supplemented with 0.05% Tween-20™. Finally, the microparticles were re-suspended in PBS and stored at 4 °C until their characterization.

Synthesis of Janus-like particles

The thermal and photo-grafted silica particles were partially masked by using wax-in-water Pickering emulsion. The emulsion was prepared by adding 20 mg of the photo-grafted particles to 100 mg of melted paraffin wax. The silica-wax solution was stirred for 10 minutes to homogeneously disperse the silica particles in the wax phase. After particles' dispersion, 2 mL of pre-heated (80 °C) and deionized water were added to the silica-wax solution. At this point, the solution was stirred at 1250 rpm at 85 °C for 30 minutes. The obtained emulsion was then cooled down to room temperature and the wax colloidosomes were collected by filtration and washed 3 times in deionized water. The prepared colloidosomes were then redispersed in water by gentle stirring (150 rpm) and irradiated by medium pressure mercury lamp at room temperature for 1 minute to cleave only the UV-exposed particles areas (intensity: UVA = 180 mW/cm^2, UVB = 32 mW/cm^2, UVC = 19 mW/cm^2, UVV 400 = mW/cm^2). The irradiated wax colloidosomes were then collected by filtration and washed 3 times in acetonitrile and then dried overnight at 45 °C in a vacuum oven. The dried colloidosomes were then dissolved in cyclohexane at 50 °C and the obtained wax-particles solution was further washed 3 times in cyclohexane and 3 times in acetone by centrifugation/redispersion cycles (3 min, 3000 rpm), in order to remove any paraffin residuals. The so obtained "Janus-irradiated" particles were then collected and dried overnight at room temperature in a vacuum oven. The subsequent coupling of the fluorescent protein onto the deprotected carboxylic acid groups of the "Janus-irradiated" particles followed the same procedure of the overall irradiated particles, as described in the previous paragraph.

Characterization methods

Thermogravimetric analysis was conducted on a thermal analyser Mettler Toledo Tga/DSC 1. The samples were heated from room temperature to 900 °C, with a heating rate of 10 K min^{-1} under air atmosphere. The mass loss, along with the residue at 900 °C, were used to evaluate the average polymer per unit area in mg of polymer per m^2 of nanoparticles surface as described elsewhere [85].

Zeta potential measurements were conducted on a Litesizer 500 particle size and zeta potential analyzer (Anton Paar GmbH, Austria). The experiments were carried out by dispersing and sonicating 12 mg of particles in 15 mL of 1 mM KCl electrolyte solution. 5 mL of the stock dispersion was further diluted in 15 mL 1 mM KCl and the zeta potential was determined as a function of the pH value. The pH value was lowered by adding HCl (30%) to the electrolyte solution and turned to higher values by adding up to 50 mM of NaOH in the electrolyte solution. For measuring the modified glass slides, a "SurPASS II" electrokinetic analyser for planar surfaces with an adjustable gap measuring cell (AGC) was used for performing the experiments. 2 samples (1 x 2 cm) were mounted in the measuring cell in a dark room. The zeta potential was determined as a function of the pH that was changed as previously described.

XPS spectra were recorded using a Thermo Fisher Scientific Instrument equipped with a monochromatic Al K-Alpha X-ray source (1486.6 eV). For the measurements, a few milligrams of the synthetized particles were placed on a carbon tape and were analyzed with a spot size of 200 µm. High resolution scans

were acquired with a pass energy of 50 eV and a step size of 0.1 eV. Survey scans were acquired with a pass energy of 200 eV and a step size of 1.0 eV. Photo electrons were collected using a take-off of 90˚ relative to the sample surface. Charge compensation was performed with an argon flood gun. All analyses were performed at 20 °C.

Ultraviolet-visible spectroscopy measurement were performed on a Lambda 950 UV/Vis/NIR Spectrometer containing a Labsphere Integrating Sphere (150 mm) to reduce light scattering from the particles. For sample preparation, the particles were dispersed in absolute ethanol (0.15 mg mL^{-1}). The measurements were carried in a wavelength range of 250 nm to 2500 nm using a dual beam method.

A microscope (Eclipse Ti2 Nikon, Tokyo, Japan) equipped with a Crest X-Light spinning disk confocal microscope and a Lumencor SPECTRA X light engine was used for the collection of fluorescence images. All images were displayed using the same scaling and were collected using a Plan Apo 20 × 0.75 NA (Nikon, Tokyo, Japan). The fluorescent images were collected on a drop of sample embedded between two cover slip microscope slides (thickness = 150 µm). The morphological characterization of the samples was carried out by field emission scanning electron microscopy (FESEM, Zeiss Supra 40). The samples were coated with a thin film of Pt/Pd 5 ηm thick.

Acknowledgements

Part of the research work was performed within the COMET-Module project “Chemitecture“ (project-no.: 21647048) at the Polymer Competence Center Leoben GmbH (PCCL, Austria) within the framework of the COMET-program of the Federal Ministry for Transport, Innovation and Technology and the Federal Ministry for Digital and Economic Affairs with contributions by Montanuniversitaet Leoben (Institute of Chemistry of Polymeric Materials). The PCCL is funded by the Austrian Government and the State Governments of Styria, Lower Austria and Upper Austria. A special acknowledgement is given to Dr. Nicolò Razza for the fruitful discussions of the results and to Dr. Annalisa Chiappone for the performed FE-SEM images.

References

1 I. J. Joye and D. J. McClements, *Curr. Opin. Colloid Interface Sci.*, 2014, **19**, 417–427.
2 I. Khan, K. Saeed and I. Khan, *Arab. J. Chem.*, 2019, **12**, 908–931.
3 J. F. Dechézelles, C. Ciotonea, C. Catrinescu, A. Ungureanu, S. Royer and V. Nardello-Rataj, *Langmuir*, 2020, **36**, 3212–3220.
4 S. Kango, S. Kalia, A. Celli, J. Njuguna, Y. Habibi and R. Kumar, *Prog. Polym. Sci.*, 2013, **38**, 1232–1261.
5 Y. Sakazaki, V. Schmitt and U. Olsson, *J. Dispers. Sci. Technol.*, 2019, **40**, 219–230.
6 N. Puretskiy and L. Ionov, *Langmuir*, 2011, **27**, 3006–3011.
7 H. Kawaguchi, *Prog. Polym. Sci.*, 2000, **25**, 1171–1210.
8 D. Vlassopoulos and G. Fytas, in *High Solid Dispersions. Advances in Polymer Science*, 2009, pp. 1–54.
9 C. Y. Li, B. Zhao and L. Zhu, *J. Polym. Sci. Part B Polym. Phys.*, 2014, **52**, 1581–1582.
10 I. Levental, P. C. Georges and P. A. Janmey, *Soft Matter*, 2007, **3**, 299–306.
11 X. Wang, V. J. Foltz, M. Rackaitis and G. G. A. Bo, *Polymer (Guildf).*, 2008, **49**, 5683–5691.
12 S. Nakayama, S. Yusa, Y. Nakamura and S. Fujii, *Soft Matter*, 2015, **11**, 9099–9106.
13 S. Minko, in *Polymer Surfaces and Interfaces*, 2008, pp. 215–234.
14 M. Sangermano and N. Razza, *Express Polym. Lett.*, 2019, **13**, 135–145.
15 J. L. M. Gonçalves, E. J. Castanheira, S. P. C. Alves, C. Baleizão and J. P. Farinha, *Polymers (Basel).*, 2020, **12**, 2175.
16 S. Tsuji and H. Kawaguchi, *Langmuir*, 2004, **20**, 2449–2455.
17 D. Roy, J. T. Guthrie and S. Perrier, *Macromolecules*, 2005, **38**, 10363–10372.
18 S. P. Le-Masurier, G. Gody, S. Perrier and A. M. Granville, *Polym. Chem.*, 2014, **5**, 2816–2823.
19 T. Shu, Q. Shen, X. Zhang and M. J. Serpe, *Analyst*, 2020, **145**, 5713–5724.
20 M. Motornov, Y. Roiter, I. Tokarev and S. Minko, *Prog. Polym. Sci.*, 2010, **35**, 174–211.
21 A. Romano, I. Roppolo, E. Rossegger, S. Schlögl and M. Sangermano, *Materials (Basel).*, 2020, **13**, 1–26.
22 C. C. Petropoulos, *J Polym Sci Polym Chem Ed*, 1977, **15**, 1637–1644.
23 C. Zhu and C. J. Bettinger, *Macromolecules*, 2015, **48**, 1563–1572.
24 O. Bertrand, E. Poggi, J. F. Gohy and C. A. Fustin, *Macromolecules*, 2014, **47**, 183–190.
25 E. Reichmanis, B. C. Smith and R. Gooden, *J. Polym. Sci. A1.*, 1985, **23**, 1–8.
26 A. M. Kloxin, A. M. Kasko, C. N. Salinas and K. S. Anseth, *Science (80-.).*, 2009, **324**, 59–63.
27 Z. Cao, Q. Li and G. Wang, *Polym. Chem.*, 2017, **8**, 6817–6823.
28 H. Zhao, W. Gu, E. Sterner, T. P. Russell, E. B. Coughlin and P. Theato, *Macromolecules*, 2011, **44**, 6433–6440.
29 H. Zhao, W. Gu, R. Kakuchi, Z. Sun, E. Sterner, T. P. Russell, E. B. Coughlin and P. Theato, *ACS Macro Lett.*, 2013, **2**, 966–969.
30 B. Mo, H. Liu, X. Zhou and Y. Zhao, *Polym. Chem.*, 2015, **6**, 3489–3501.
31 C. Liu, K. K. Ewert, W. Yao, N. Wang, Y. Li, C. R. Safinya and W. Qiao, *ACS Appl. Mater. Interfaces*, 2020, **12**, 70–85.
32 W. Li, Y. G. He, S. Y. Shi, N. Liu, Y. Y. Zhu, Y. S. Ding, J. Yin and Z. Q. Wu, *Polym. Chem.*, 2015, **6**, 2348–2355.
33 L. Li, J. M. Scheiger and P. A. Levkin, *Adv. Mater.*, 2019, **31**, 1807333.
34 M. Hegazy, P. Zhou, N. Rahoui, G. Wu, N. Taloub, Y. Lin, X. Huang and Y. Huang, *Colloids Surfaces A Physicochem. Eng.*

Asp., 2019, **581**, 123797.
35 D. Han, X. Tong and Y. Zhao, *Langmuir*, 2012, **28**, 2327–2331.
36 Y. Z. Wang, L. Li, F. S. Du and Z. C. Li, *Polymer (Guildf).*, 2015, **68**, 270–278.
37 A. Del Campo, D. Boos, H. W. Spiess and U. Jonas, *Angew. Chemie - Int. Ed.*, 2005, **44**, 4707–4712.
38 C. E. J. Cordonier, A. Nakamura, K. Shimada and A. Fujishima, *Langmuir*, 2012, **28**, 13542–13548.
39 J. A. Shadish, G. M. Benuska and C. A. DeForest, *Nat. Mater.*, 2019, **18**, 1005–1014.
40 J. S. Katz, J. Doh and D. J. Irvine, *Langmuir*, 2006, **22**, 353–359.
41 P. Gumbley, D. Koylu, R. H. Pawle, B. Umezuruike, E. Spedden, C. Staii and S. W. Thomas, *Chem. Mater.*, 2014, **26**, 1450–1456.
42 X. Hu, Z. Qureishi and S. W. Thomas, *Chem. Mater.*, 2017, **29**, 2951–2960.
43 T. Konishi, T. Hashimoto, N. Sato, K. Nakajima and K. Yamaguchi, *Bull. Chem. Soc. Jpn.*, 2016, **89**, 125–134.
44 J. A. Bardecker, A. Afzali, G. S. Tulevski, T. Graham, J. B. Hannon and A. K. Y. Jen, *Chem. Mater.*, 2012, **24**, 2017–2021.
45 P. Wei, B. Li, A. De Leon and E. Pentzer, *J. Mater. Chem. C*, 2017, **5**, 5780–5786.
46 M. Edler, S. Mayrbrugger, A. Fian, G. Trimmel, S. Radl, W. Kern and T. Griesser, *J. Mater. Chem. C*, 2013, **1**, 3931–3938.
47 E. Rossegger, D. Hennen, T. Griesser, I. Roppolo and S. Schlögl, *Polym. Chem.*, 2019, **10**, 1882–1893.
48 E. Rossegger, D. Nees, S. Turisser, S. Radl, T. Griesser and S. Schlögl, *Polym. Chem.*, 2020, **11**, 3125–3135.
49 A. Romano, A. Angelini, E. Rossegger, G. Palmara, M. Castellino, F. Frascella, A. Chiappone, A. Chiadò, M. Sangermano, S. Schlögl and I. Roppolo, 2020, **2000084**, 1–7.
50 M. Giebler, S. V. Radl, M. Ast, S. Kaiser, T. Griesser, W. Kern and S. Schlögl, *J. Polym. Sci. Part A Polym. Chem.*, 2018, **56**, 2319–2329.
51 M. Giebler, S. Radl, T. Ules, T. Griesser and S. Schlögl, *Materials (Basel).*, 2019, **12**, 2350.
52 S. Radl, I. Roppolo, K. Pölzl, M. Ast, J. Spreitz, T. Griesser, W. Kern, S. Schlögl and M. Sangermano, *Polymer (Guildf).*, 2017, **109**, 349–357.
53 S. V. Radl, C. Schipfer, S. Kaiser, A. Moser, B. Kaynak, W. Kern and S. Schlögl, *Polym. Chem.*, 2017, **8**, 1562–1572.
54 S. Radl, M. Kreimer, J. Manhart, T. Griesser, A. Moser, G. Pinter, G. Kalinka, W. Kern and S. Schlögl, *Polymer (Guildf).*, 2015, **69**, 159–168.
55 P. Alonso-Cristobal, O. Oton-Fernandez, D. Mendez-Gonzalez, J. F. Díaz, E. Lopez-Cabarcos, I. Barasoain and J. Rubio-Retama, *ACS Appl. Mater. Interfaces*, 2015, **7**, 14992–14999.
56 P. Picchetti, B. N. Dimarco, L. Travaglini, Y. Zhang, M. C. Ortega-Liebana and L. De Cola, *Chem. Mater.*, 2020, **32**, 392–399.
57 J. Lee, K. H. Ku, J. Kim, Y. J. Lee, S. G. Jang and B. J. Kim, *J. Am. Chem. Soc.*, 2019, **141**, 15348–15355.
58 H. Li, H. Zheng, Y. Zhang, W. Zhang, W. Tong and C. Gao, *J. Colloid Interface Sci.*, 2018, **514**, 182–189.
59 N. Vilanova, I. De Feijter, A. J. P. Teunissen and I. K. Voets, *Sci. Rep.*, 2018, **8**, 1–9.
60 B. Lin and S. Zhou, *Appl. Surf. Sci.*, 2015, **359**, 380–387.
61 N. Razza, G. Rizza, P. E. Coulon, L. Didier, G. C. Fadda, B. Voit, A. Synytska, H. Grützmacher and M. Sangermano, *Nanoscale*, 2018, **10**, 14492–14498.
62 M. Sangermano, M. Periolatto, M. Castellino, J. Wang, K. Dietliker, J. L. Grützmacher and H. Grützmacher, *ACS Appl. Mater. Interfaces*, 2016, **8**, 19764–19771.
63 N. Razza, M. Castellino and M. Sangermano, *J. Mater. Sci.*, 2017, **52**, 13444–13454.
64 A. Kirillova, C. Marschelke and A. Synytska, *ACS Appl. Mater. Interfaces*, 2019, **11**, 9643–9671.
65 H. Su, C. H. Price, L. Jing, Q. Tian, J. Liu and K. Qian, *Mater. Today Bio*, 2019, **4**, 100033.
66 A. Walther and A. H. E. Mu, *Chem. Rev.*, 2013, **113**, 5194–5261.
67 L. Hong, S. Jiang and S. Granick, *Langmuir*, 2006, **22**, 9495–9499.
68 S. Campuzano and J. M. Pingarrón, *Appl. Mater. Today*, 2017, **9**, 276–288.
69 B. Liu, W. Wei, X. Qu and Z. Yang, *Angew. Chemie*, 2008, **47**, 3973–3975.
70 A. Huber, A. Kuschel, T. Ott, G. Santiso-Quinones, D. Stein, J. Bräuer, R. Kissner, F. Krumeich, H. Schönberg, J. Levalois-Grützmacher and H. Grützmacher, *Angew. Chemie - Int. Ed.*, 2012, **51**, 4648–4652.
71 M. Sahin, K. K. Krawczyk, P. Roszkowski, J. Wang, B. Kaynak, W. Kern, S. Schlögl and H. Grützmacher, *Eur. Polym. J.*, 2018, **98**, 430–438.
72 M. Sahin, S. Schlögl, S. Kaiser, W. Kern, J. Wang and H. Grützmacher, *J. Polym. Sci. Part A Polym. Chem.*, 2017, **55**, 894–902.
73 G. W. Sluggett, P. F. McGarry, I. V. Koptyug and N. J. Turro, *J. Am. Chem. Soc.*, 1996, **118**, 7367–7372.
74 A. A. Eibel, D. E. Fast, J. Sattelkow, J. Wang, A. Huber, G. Müller, D. Neshchadin, K. Dietliker, H. Plank, H. Grützmacher and G. Gescheidt, *Angew. Chemie - Int. Ed.*, 2017, **56**, 14306–14309.
75 S. Jockusch and N. J. Turro, *J. Am. Chem. Soc.*, 1998, **120**, 11773–11777.
76 J.-F. G. Jean-Marc Schumers, Charles-Andrè Fustin, Aydin Can, Richard Hoogenboom, Ulrich S. Schubert, *J. Polym. Sci. Part A Polym. Chem.*, 2009, **47**, 6504–6513.
77 E. M. Muzammil, A. Khan and M. C. Stuparu, *RSC Adv.*, 2017, **7**, 55874–55884.
78 A. K. Singh, B. P. Panda, S. Mohanty, S. K. Nayak and M. K. Gupta, *Korean J. Chem. Eng.*, 2017, **34**, 3028–3040.
79 H.-J. Jacobasch and J. Schurz, *Dispersed Syst.*, 2007, **48**, 40–48.
80 P. Xu, H. Wang, R. Tong, Q. Du and W. Zhong, *Colloid Polym. Sci.*, 2006, **284**, 755–762.
81 D. Briggs and G. Beamson, *Anal. Chem.*, 1992, **64**, 1729–1736.

82 J. S. Stevens, C. R. Seabourne, C. Jaye, D. A. Fischer, A. J. Scott and S. L. M. Schroeder, *J. Phys. Chem. B*, 2014, **118**, 12121–12129.
83 C. Luo, X. Ji, S. Hou, N. Eidson, X. Fan, Y. Liang, T. Deng, J. Jiang and C. Wang, *Adv. Mater.*, 2018, **30**, 1–9.
84 A. Chiadò, G. Palmara, S. Ricciardi, F. Frascella, M. Castellino, M. Tortello, C. Ricciardi and P. Rivolo, *Colloids Surfaces B Biointerfaces*, 2016, **143**, 252–259.
85 J. P. Gann and M. Yan, *Langmuir*, 2008, **24**, 5319–5323.